

Modelling the interaction between relativistic and non-relativistic winds in binary pulsar systems: strong magnetization of the pulsar wind

S.V.Bogovalov¹, D.Khangulyan^{2*}, A.Koldoba³, G.V.Ustyugova⁴, F.Aharonian^{5,6,1}

¹*National Research Nuclear University (MEPhI), Kashirskoe shosse, 31, Moscow, Russia*

²*Rikkyo University, 3-34-1, Nishi-Ikebukuro, Toshima-ku, Tokyo 171-8501, Japan*

³*Moscow institute of physics and technology, Institutskiy per. 9, Dolgoprudny, Russia*

⁴*Keldysh Institute of Applied Mathematics RAN, Miusskaya sq. 4, Moscow, Russia*

⁵*Dublin Institute for Advanced Studies, School of Cosmic Physics, 31 Fitzwilliam Place, Dublin 2, Ireland*

⁶*Max-Planck-Institut für Kernphysik, Saupfercheckweg 1, 69117 Heidelberg, Germany*

ABSTRACT

We present a numerical study of the properties of the flow produced by the collision of a magnetized anisotropic pulsar wind with the circumbinary environment. We focus on studying the impact of the high wind magnetization on the geometrical structure of the shocked flow. This work is an extension of our earlier studies that focused on a purely hydrodynamic interaction and weak wind magnetization. We consider the collision in the axisymmetric approximation, that is, the pulsar rotation axis is assumed to be oriented along the line between the pulsar and the optical star. The increase of the magnetization results in the expansion of the opening cone in which the shocked pulsar wind propagates. This effect is explained in the frameworks of the conventional theory of collimation of magnetized winds. This finding has a direct implication for scenarios that involve Doppler boosting as the primary mechanism behind the GeV flares detected with the *Fermi* Large Area Telescope from PSR B1259–63/LS2883. The maximum enhancement of the apparent emission is determined by the ratio of 4π to the solid in which the shocked pulsar wind propagates. Our simulations suggest that this enhancement factor is decreased by the impact of the magnetic field.

Key words: pulsars, magnetohydrodynamics, binary system

1 INTRODUCTION

Several binary systems, e.g., PSR B1259–63/LS2883 (PSR B1259), LS 5039, 1FGL J1018.6–5856, LSI+61°303, and LMC P3 emit bright non-thermal emission that spans across the entire electromagnetic spectrum, from radio to gamma-ray energies (see, e.g., [Dubus 2013](#), and references therein). These systems are detected with ground-based Cherenkov detectors, H.E.S.S., MAGIC, and *Veritas* in the very-high-energy (VHE) regime and with the *Fermi* Large Area Telescope (*Fermi* LAT) at high energies (HE) (see, e.g., [Corbet et al. 2016, 2019](#); [Bordas et al. 2017](#); [Maier & VERITAS Collaboration 2017](#); [López-Oramas et al. 2018](#), and references therein). The spectral maximum typically appears at MeV–GeV energies. The emission detected from these systems shows a complex orbital phase dependence that yet have not obtained a detailed explanation.

In analogy to binary systems bright in the X-ray band,

these systems were lumped together into a new class of gamma-ray binary system (GRBS). While two GRBSs, PSR B1259 and PSR J2032+4127/MT91 213, harbor confirmed radio pulsars ([Johnston et al. 1992](#); [Lyne et al. 2015](#)), the nature of the compact objects in other GRBSs is not constrained observationally. Because of spectral similarities, it is commonly assumed that all GRBSs consist of non-accreting pulsars orbiting luminous stars ([Dubus 2006b](#)). The interaction of the winds from the pulsar and the optical companion presumably triggers particle acceleration and consequent non-thermal emission ([Maraschi & Treves 1981](#); [Tavani et al. 1994](#); [Martocchia et al. 2005](#)). We note here that some binary systems detected in HE or even in the VHE regime do not belong to the class of GRBS. The gamma-ray emission detected from Galactic microquasar Cygnus X-1, Cygnus X-3, and SS 433/W50 constitutes a small fraction, $< 10\%$, of the bolometric luminosity of the sources, and most-likely originates in the jets ([Dubus et al. 2010](#); [Zanin et al. 2016](#); [Zdziarski et al. 2018](#); [Abeysekara et al. 2018](#); [Xing et al.](#)

* E-mail: d.khangulyan@rikkyo.ac.jp

2019) or even in the jet termination region (Bordas et al. 2015).

Gamma-ray emission was also detected from colliding-wind binaries (CWBs), i.e., systems where two stars with powerful winds orbit each other. CWBs are well-established sources of non-thermal emission (Eichler & Usov 1993; De Becker & Rauq 2013; Hamaguchi et al. 2018). In the case of extended CWB, e.g. WR 140 (a WR+O binary system, see Dougherty et al. 2005a,b), radio observations allowed us to localize the acceleration site that appeared to be between the stars, where the wind interaction is the most intense. One of the most extreme CWB, η Carinae has been also detected as a gamma-ray source with *Fermi* LAT (Abdo et al. 2010; Reitberger et al. 2015) and H.E.S.S. (Leser et al. 2017). The detected non-thermal emission from CWB is consistent with models accounting for the particle acceleration at wind termination shocks and advection (Reitberger et al. 2014). When non-thermal particles move along the flow they lose energy due to synchrotron, inverse Compton (IC), and hadronic (in case of non-thermal protons) emission mechanisms. Adiabatic cooling may also play an important role. As a result, non-thermal particles have a complex spacial-energy distribution. Convolution of this distribution with target fields, which in turn also have a highly non-homogeneous anisotropic distribution, allows us to compute the broadband emission spectra and lightcurves (Reitberger et al. 2014).

In the framework of the rotation-powered pulsar scenario, GRBSs represent a version of CWB, where one of the winds is ultrarelativistic. The relativistic nature of the pulsar wind implies important hydrodynamic (HD) differences between CWBs and GRBSs (Bosch-Ramon et al. 2012). Since the regular CWBs appear to be significantly less efficient non-thermal emitters as compared to GRBSs, it is natural to attribute the dominant non-thermal activity in GRBSs to processes taking place in the pulsar wind. Thus, GRBSs were considered as compactified pulsar wind nebula (PWN) located in an environment with an unusually dense photon field (see, e.g., Tavani et al. 1994; Kirk et al. 1999; Chernyakova & Illarionov 1999; Bosch-Ramon & Barkov 2011). However, detailed HD and magneto-HD (MHD) simulations revealed critical differences as compared to (M)HD processes taking place around isolated pulsars (Bogovalov et al. 2008, 2012). Certain similarities can be seen between binary pulsars and PWNe around bow-shock pulsars, which propagate through interstellar medium (ISM) with a supersonic proper speed. This, however, concerns only the region close to the head of the bow shock. At large distances from the apex point, the structure of the flow starts to deviate considerably. In the case of binary pulsars the ram pressure of the stellar and pulsar winds decreases at large distance allowing an opened pulsar wind zone (Bogovalov et al. 2008). For bow-shock nebulae, the ram pressure of ISM remains constant, which results in a closed pulsar wind zone.

Theoretical studies (Eichler & Usov 1993; Wilkin 1996) and numerical simulations (Romero et al. 2007; Bogovalov et al. 2008, 2012; Okazaki et al. 2011; Lamberts et al. 2013) of colliding winds revealed that the shocked flow propagates into a limited solid angle on the binary system scale. The interaction of two winds results in re-acceleration of shocked pulsar wind to relativistic speeds (Bogovalov et al. 2008, 2012; Bosch-Ramon et al. 2012; Lamberts et al. 2013). The

shocked pulsar wind material reaches relativistic bulk speeds on the characteristic binary separation scale. The relativistic motion may have a strong impact on the production of non-thermal emission, and result in complicated time variability patterns (Kong et al. 2012; Khangulyan et al. 2014; de la Cita et al. 2017). This might be the key factor that explains the complex orbital phase dependence of the non-thermal emission seen from GRBSs. In particular, Doppler boosting seems to be the most natural explanation for the emission with a luminosity exceeding the pulsar spindown losses seen from PSR B1259 with *Fermi* LAT during the GeV flare registered in 2017 (Johnson et al. 2018; Chang et al. 2018), which becomes even more significant with the increased estimate for the distance to the source (Miller-Jones et al. 2018).

The impact of Doppler boosting on the emission critically depends on two factors: the fluid bulk Lorentz factor and the solid angle, $\Delta\Omega$, subtended by the outflow. Since the flow bulk acceleration proceeds because of a HD process, the increase of the bulk Lorentz factor is accomplished by the severe adiabatic cooling of the plasma. Thus, the impact of the high bulk Lorentz factor on the emission intensity depends on the radiation mechanism, and might be even counterintuitive: the synchrotron emissivity is expected to be severely weakened by the bulk acceleration (Khangulyan et al. 2014). Thus, the solid angle into which the shocked pulsar wind propagates may have a dominant impact on the emission intensity.

In the previous works (Bogovalov et al. 2008, 2012) we considered the collision of the stellar and pulsar winds in the specific cases of non-magnetized and weakly magnetized pulsar winds. The calculations were performed for an axisymmetric 2D geometry. In this case, the rotational axis of the pulsar is aligned with the line connecting the pulsar and the companion star. Re-acceleration of the post-shock flow results in a rapid weakening of the magnetic field. Thus, there should be very little differences in the interaction geometry in the cases of non-magnetized and weakly magnetized pulsar winds colliding with the stellar wind. The geometry of the structure formed on the binary system scale depends on the ratio of the winds' ram pressures (for details, see Bogovalov et al. 2008). The magnetic field weakening makes it to be dynamically unimportant allowing us to generalize our conclusion to the case of the arbitrary orientation of the pulsar rotation axis.

We note, however, that the kinetic energy flux in the pulsar wind is expected to be highly anisotropic (Bogovalov & Khangoulia 2002), thus realistic calculations demand a 3D setup. Also 3D simulations are needed to account for orbital motion in the system (Romero et al. 2007; Okazaki et al. 2011; Bosch-Ramon et al. 2015), although certain conclusions also can be obtained with 2D approaches (Bosch-Ramon et al. 2012; Barkov & Bosch-Ramon 2016; Bosch-Ramon et al. 2017; Barkov & Bosch-Ramon 2018).

The results obtained by Bogovalov et al. (2012) show a qualitative difference between binary pulsars and PWN created by isolated pulsars. In the latter case, the magnetic field strength increases in the shocked pulsar wind until magnetic stresses become dynamically important (Kennel & Coroniti 1984). The simulations presented by Bogovalov et al. (2012) concern however only the case of a weakly magnetized pulsar wind, a property that is expected based on one-dimensional and 2D MHD consideration of PWN (Kennel & Coroniti

1984; Bogovalov & Khangoulia 2002; Khangoulia & Bogovalov 2003; Bogovalov et al. 2005; Del Zanna et al. 2004). A recent 3D numerical simulation relaxes the requirement for a small magnetization in pulsar winds (Porth et al. 2014; Olmi et al. 2016). If the magnetic field is strong at the pulsar wind termination shock then it may appear to be dynamically important even in the case of an accelerating bulk flow. The toroidal magnetic field, which is expected to be present in the pulsar wind, can lead to in the collimation of the outflow provided that the magnetic field is sufficiently strong (Bogovalov & Tsinganos 1999). Studying the possibility of such a collimation is essential for the interpretation of the complicated orbital phase dependence seen from GRBS. In this paper we extend the previous studies (Bogovalov et al. 2008, 2012) to the case of a strongly magnetized pulsar wind. We limit our consideration to the axisymmetric case. In such a configuration, the preferred directions for the HD and the magnetic collimation coincide, so one may expect the strongest collimation effect.

As our benchmark case, we consider GRBS PSR B1259. The system consists of a ~ 47.8 ms pulsar in an elongated orbit, with eccentricity $e = 0.87$, around a massive O-type companion (Johnston et al. 1992; Negueruela et al. 2011; Shannon et al. 2014; Miller-Jones et al. 2018). During the last 25 years this system was observed with different instruments in radio frequencies (Johnston et al. 1994, 1996, 2005; Moldón et al. 2011; Shannon et al. 2014; Fujita et al. 2019), optical wavelengths (Negueruela et al. 2011; van Soelen et al. 2016), in the X-ray band (Kaspi et al. 1995; Murata et al. 2003; Uchiyama et al. 2009; Chernyakova et al. 2006, 2009, 2014, 2015; Pavlov et al. 2011, 2015), GeV gamma rays (Abdo et al. 2011; Caliendo et al. 2015; Chang et al. 2018; Johnson et al. 2018), and in the VHE regime (Aharonian et al. 2005, 2009; Abramowski et al. 2013). The detected emission consists of several components: the optical and infrared emission from the massive companion and its decretion disk, pulsed radio emission, and a variable broadband component that presumably is produced by non-thermal electrons accelerated at the interface between the stellar and the pulsar wind (see also Zabalza et al. 2013, where one considered non-thermal particles accelerated at the termination shock caused by the impact of the Coriolis force in the same kind of scenario).

2 MODEL SETUP AND SIMULATION RESULTS

In the simplest case, if one approximates both the stellar and the pulsar winds by isotropic non-magnetized outflows, the flow formed at the winds' collision features axial symmetry (Bogovalov et al. 2008). To simulate the interaction of a magnetized pulsar wind, the calculations should be performed in a 3D setup (see, e.g., Bandiera 1993; Wilkin 2000), or one needs to adopt an additional assumption that the pulsar rotation axis and the line connecting interacting stars are parallel. This assumption is not critical in the case of a weak pulsar wind magnetization (Bogovalov et al. 2012). However, in the case of a high wind magnetization, this might be a rather artificial conjecture. We nevertheless adopt this configuration for our simulations. The reason for that is the following: we aim to study the maximum possible collima-

tion of the shocked pulsar wind by the magnetic field. This is achieved in the axisymmetric setup. To perform the numerical simulation, we use a mathematical model and numerical algorithm, which are summarized in Koldoba et al. (2019).

2D axisymmetric solution can be significantly affected by the Coriolis force at some distance from the collision apex (Bosch-Ramon & Barkov 2011). The typical distance at which the pulsar trace bends significantly can be easily estimated in the limit $\eta \ll 1$. The shocked material follows in this case a spiral trajectory, which in polar coordinates, (r, ϕ) , is defined as

$$r(\phi) = D + v_w \phi / \omega. \quad (1)$$

Here ω is the orbital angular velocity of the pulsar, v_w is the stellar wind radial velocity, and D is the star separation distance. Close to the pulsar location, $\phi = 0$, the curvature of this trajectory is

$$R_c = r \frac{\left(1 + \left(\frac{r'}{r}\right)^2\right)^{3/2}}{1 + 2\left(\frac{r'}{r}\right)^2 - \left(\frac{r''}{r}\right)} \simeq D \frac{v_w}{2v_{\text{orb}}}, \quad (2)$$

where v_{orb} is the orbital velocity of the pulsar. Thus, the dimensionless size of the region, where the trace bending is negligible is $z \simeq R_c/D \simeq v_w/(2v_{\text{orb}})$. For the conditions typical in GRBS, this corresponds to $z \simeq 5$, consistently with the size of the region where the impact of the orbital motion is small as obtained with numerical simulations (see, e.g., Bosch-Ramon et al. 2012).

Under the approximation of axisymmetry, the flow is characterized by two parameters. The first parameter is the ratio of the momentum rates of the pulsar and stellar winds. Although the pulsar spindown losses are distributed between Poynting and kinetic energy, we still introduce this parameter in a form that accounts only for the kinetic energy, whose flux is assumed to be isotropic:

$$\eta = \frac{\dot{M} c \gamma_0}{\dot{M}_* v_w}, \quad (3)$$

where \dot{M} and \dot{M}_* are the mass-loss rates of the pulsar and the optical star, respectively. At the collision distance, and the pulsar wind is assumed to have a bulk Lorentz factor of γ_0 . In the case of PSR B1259, one expects that the η -parameter is in the range 0.2 – 0.6 if the pulsar interacts with the polar wind (Bogovalov et al. 2008). The impact of the η -parameter has been extensively studied in our previous works (Bogovalov et al. 2008, 2012). In what follows we adopt a fixed value for this parameter, $\eta = 0.3$. In the case of a purely hydrodynamic interaction, one should expect the following configuration: the opening angles of the relativistic termination shock and the contact discontinuity are $\sim 50^\circ$ and $\sim 70^\circ$, respectively (see Fig.11 in Bogovalov et al. 2008). The comparison with this geometry, characterized by the opening angles close to 60° , should allow us to study the impact of magnetic field.

If the η -parameter is small, $\eta \ll 1$, the location of the contact discontinuity (i.e., the surface that separates the shocked relativistic and non-relativistic winds) on the line connecting the stars is defined as follows (Bogovalov et al. 2008):

$$r_{\text{CD}} \approx \sqrt{\eta}. \quad (4)$$

Here, r_{CD} is the distance to the pulsar expressed in units of the star separation distance.

Another parameter that determines the flow structure is the pulsar wind maximum magnetization, σ . Since the magnetic field in the pulsar wind is expected to be toroidal, the Poynting flux along the symmetry axis vanishes. We assume the total energy flux from the pulsar to be:

$$\frac{dL_{\text{PSR}}}{d\Omega} = \frac{\gamma_0 \dot{M} c^2}{4\pi} (1 + \sigma \sin^2(\theta)), \quad (5)$$

where θ is the polar angle and the solid angle element is $d\Omega = \sin \theta d\phi d\theta$. This allows us to express the σ -parameter as

$$\sigma = \frac{3}{2} \left(\frac{L_{\text{PSR}}}{\gamma_0 \dot{M} c^2} - 1 \right). \quad (6)$$

Here, L_{PSR} is the spindown luminosity of the pulsar. In the simulations, we keep the parameters of the stellar wind and the kinetic energy flux of the pulsar wind to be fixed. Thus, the increase of the sigma parameter results in a change of the pulsar spindown losses, L_{PSR} .

We are now interested in the range of $\sigma = 0.1 - 1$, which extends the case of small magnetization, $\sigma < 0.1$, presented in Bogovalov et al. (2012), to the range of the magnetization consistent with 3D simulations (Porth et al. 2014; Olmi et al. 2016).

Numerical simulations of the flow geometry and the bulk Lorentz factor are shown in Figs. 1, 2, and 3 for $\sigma = 0$, 0.5, and 0.8, respectively ($\eta = 0.3$ was fixed for all three cases). The spatial coordinates are dimensionless in the star separation units. The optical star and the pulsar are located at the points with coordinates $(r = 0, z = 1)$ and $(r = 0, z = 0)$, respectively. Qualitatively the flow structure is identical to those revealed with other simulations (Bogovalov et al. 2008, 2012; Bosch-Ramon et al. 2012, 2015). Supersonic winds propagate from the stars until reaching bow-shaped termination shocks, which are marked in the figures with symbols “R” and “N” (relativistic pulsar wind termination shock and non-relativistic stellar wind termination shock, respectively). The supersonic flows are not shown in the figures. The volume between the termination shocks is filled with shocked gas. A contact discontinuity, which is marked with symbol “C” in the figures, separates the relativistic and the non-relativistic gas. The shocked nonrelativistic plasma originated from the companion star propagates in the cone “NC,” and the shocked relativistic plasma in the cone “CR.”

From a comparison of the figures it can be seen that the increasing wind magnetization has a considerable impact on the flow geometry. The region occupied by the shocked pulsar wind expands significantly. This phenomena is accompanied by a decrease of the bulk Lorentz factor. After passage of the termination shock, a fraction of the kinetic energy is transformed into Poynting flux that results in a decrease of the Lorentz factor of the shocked wind.

In Fig. 4, we show the dependence of the opening angles of the relativistic termination shock and the contact discontinuity on σ . The opening angle of the contact discontinuity increases and the opening angle of the relativistic termination shock decreases with σ . This results in a significant expansion of the region occupied by the shocked winds. According to Eq. (5), the increase of σ results into growth of

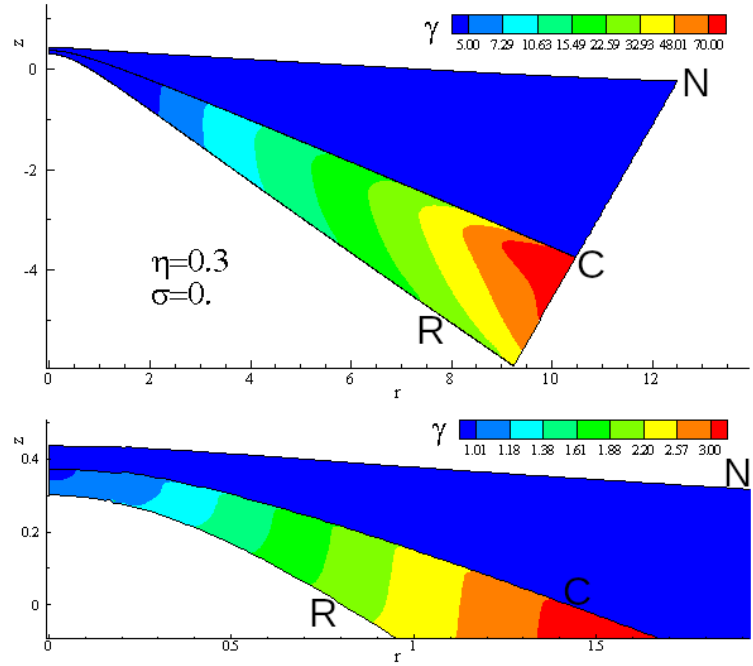


Figure 1. Shocked flow of plasma from the companion star (in the cone NC) and the pulsar (in the cone RC) for $\sigma = 0$ and $\eta = 0.3$. The radial flows of the supersonic plasma from the companion star (located at the point (0,1)) and the pulsar (located at the point (0,0)) upstream of the shocks are not shown. The flows of the non-relativistic and relativistic plasma in the post shock region are separated by the contact discontinuity (line C). The color in the region of the flow of the shocked relativistic plasma shows the Lorentz factor of the plasma. Panels show a large-scale structure and a zoomed view of the inner part of the binary system.

the actual total pulsar energy losses. The flux of the kinetic energy remains constant. If there were no impact from the magnetic collimation, one would expect that the impact on the flow structure can be approximately determined by the effective change η -parameter:

$$\eta_{\text{eff}} = \eta \left(1 + \frac{2}{3} \sigma \right). \quad (7)$$

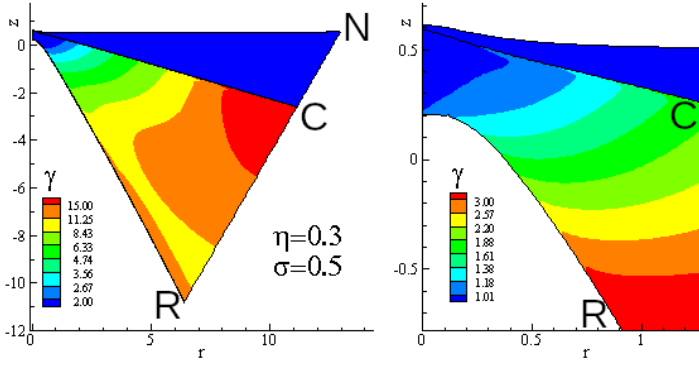
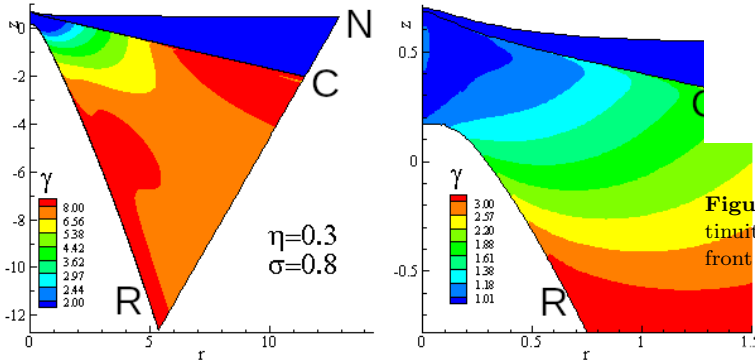
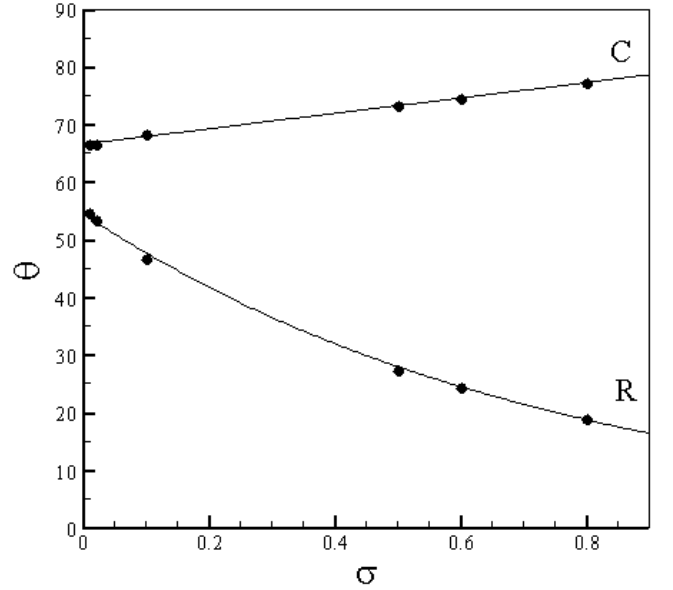
In the regime $\eta_{\text{eff}} > 10^{-2}$, the opening angle of the contact discontinuity can be approximately described (see Fig.11 in Bogovalov et al. 2008) as:

$$\theta_{\text{CD}} \approx 85^\circ + 15^\circ \ln \eta_{\text{eff}} \approx 67^\circ + 10^\circ \sigma, \quad (8)$$

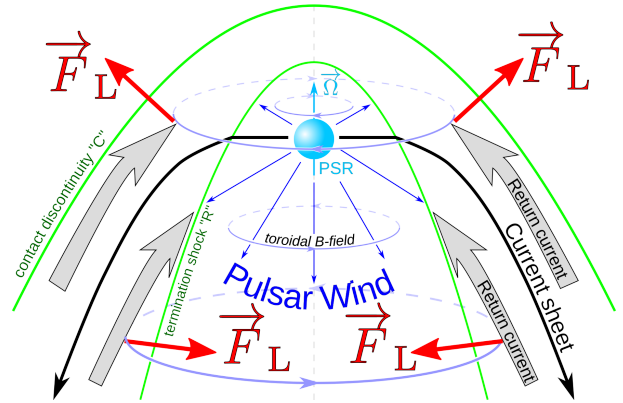
where we used $\eta = 0.3$. Thus, the increase of the opening angle of the contact discontinuity seen in Fig. 4 is consistent with the change of the pulsar spindown power due to the contribution from Poynting flux. Based on result from Bogovalov et al. (2008), one should also expect an increase of the pulsar wind termination shock as the σ -parameter grows. In contrast, as seen in Fig. 4 the opening angle of the pulsar wind termination shock is decreasing.

3 DISCUSSION

Numerical simulations of the interaction of the magnetized pulsar wind with the isotropic stellar wind under the ap-


 Figure 2. Same as in Fig.1 for $\sigma = 0.5$.

 Figure 3. Same as in Fig.1 for $\sigma = 0.8$.

 Figure 4. Dependence of the opening angle of the contact discontinuity (marked with “C”) and the relativistic termination shock front (marked with “R”) on σ .

proximation of axisymmetry show that the wind magnetization has a strong impact on the interaction geometry in the regime $\sigma \sim 1$. As shown in Fig. 4, the solid angle occupied by the shocked pulsar wind tends to increase considerably with increasing σ . The reason of this dependence can be qualitatively understood as the Lorentz force impact (see, e.g., Kalapotharakos et al. 2012). In Fig. 5, we show a scheme showing the structure of the relativistic outflow. For the sake of simplicity, we assumed that the pulsar magnetic axis coincides with the rotation axis. The magnetic and rotational axes of the pulsar are aligned along the pulsar-star connecting line. In the unshocked wind zone, the current sheet, i.e., the surface that separates regions of opposite polarity toroidal magnetic field (shown with a solid black line in Fig. 5), lies on the equatorial plane, which is perpendicular to the symmetry axis. The current sheet propagates through the termination shock, but gets deflected in the shocked relativistic plasma. The electric currents propagate through the shocked pulsar wind above and below the current sheet as shown in Fig. 5. Since the polarity of the magnetic field below and above the current sheet changes, the Lorentz force is directed differently. Therefore, the collimating force above the current sheet is directed towards the contact discontinuity and creates an additional pressure on it. This contributes to the growth of the contact discontinuity opening angle. The collimating force below the current


 Figure 5. Scheme of the flow of the relativistic plasma. The Lorentz force, \vec{F}_L , extends the cone of the contact discontinuity (C) and collimates the relativistic shock wave (R).

sheet is directed towards the pulsar wind termination shock front. Consequently, the termination shock is pushed closer to the symmetry axis.

Although we considered a rather specific case, in which the rotation and magnetic axes of the pulsar are aligned with the symmetry axis, a similar argument seems to be valid in a more general case. At large distances, pulsar winds practically do not differ from the winds launched by a split monopole magnetic field (Kalapotharakos et al. 2012). The distribution of magnetic pressure in the flow from a split monopole does not depend on the orientation of the magnetic axis (Michel 1973; Bogovalov 1999). Thus, the struc-

ture of the Lorentz force should remain unchanged independently on the orientation of the pulsar magnetic axis.

The influence of the orientation of the rotation axis needs to be studied in the 3D approximation (see, e.g., the study by [Barkov et al. 2019a,b](#); [Olmi & Bucciantini 2019](#), for the case of bow-shock PWN). To consider such a configuration in a binary system, additional studies are required, which are, however, beyond the scope of this paper.

GRBS represent a class of gamma-ray sources where MHD processes are expected to play an essential role. Broad-band non-thermal components observed from these systems are most likely produced in the shocked pulsar wind. Thus, one expects important similarities between GRBSs and PWNe (see, e.g., [Tavani et al. 1994](#); [Kirk et al. 1999](#); [Khangulyan et al. 2007](#)). There are, however, also important differences that include a significantly smaller scale, the presence of dense photon target field, and gradual changes of the physical conditions due to orbital motion. The high pressure as well as the dense photon target field reduce the relevant space- and time-scales by many orders of magnitude, allowing one to study the processes taking place in PWNe under varying conditions and on much shorter time scales. GRBS can be considered as essential physical laboratories to study the physics of PWN.

The strong orbital phase dependence of the emission is expected to be caused by several factors. In particular this includes the following: (i) anisotropic IC scattering of target photons provided by the optical companion ([Khangulyan et al. 2008](#); [Dubus et al. 2008](#)), (ii) changing rate of adiabatic and radiative losses ([Kirk et al. 1999](#); [Khangulyan et al. 2007](#)), (iii) orbital phase depended gamma-gamma attenuation ([Böttcher & Dermer 2005](#); [Dubus 2006a](#)), (iv) Doppler boosting caused by bulk re-acceleration of the shocked pulsar wind ([Kong et al. 2012](#); [Khangulyan et al. 2014](#)). The latter factor is of special interest, as this is the only factor that can enhance the source apparent luminosity above the limit determined by the spindown luminosity. Importantly, observations of PSR B1259 with *Fermi* LAT have shown that the gamma-ray flux level may increase above this limit (see the discussion in [Caliandro et al. 2015](#); [Johnson et al. 2018](#); [Miller-Jones et al. 2018](#)). Such a detection makes models that do not involve Doppler boosting less feasible (e.g., [Khangulyan et al. 2012](#); [Dubus & Cerutti 2013](#)). However, in the context of GRBS, the Doppler boosting affects the synchrotron and IC components in a very different way (see, e.g., [Khangulyan et al. 2014](#)). The weakening of the magnetic field, which is expected in accelerating flow, suppresses the synchrotron emission. Thus, Doppler boosting can considerably enhance only the IC emission. Note however that, since the dominant photon target is provided by the optical companion, the enhancement factor is different compared to those obtained for blob sources (see, e.g., [Khangulyan et al. 2018](#)).

Doppler boosting in GRBS critically depends on the solid angle into which the shocked pulsar wind propagates. [Bogovalov et al. \(2008\)](#) obtained analytic approximations that allows us to describe the flow geometry in the case of weak magnetization of the pulsar wind. Significant collimation, $4\pi/\Delta\Omega > 10$, can be achieved only in the cases of small η parameters ($\eta < 0.05$), which implies an unrealistically powerful stellar wind. In this paper, we studied the impact of a high wind magnetization on the collimation

of the shocked pulsar wind. Our simulation indicates that higher values of the σ -parameter, $\sigma \sim 1$, even result in further de-collimation of the shocked pulsar wind. This finding is consistent with the conventional theories of the dynamics of magnetized outflows. We therefore conclude that the de-collimation is caused by physical reasons and it is unlikely to be a numerical artifact. This challenges the scenarios that adopt Doppler boosting as the main mechanism responsible for production of GeV flares detected with *Fermi* LAT from PSR B1259.

In this paper we performed numerical simulations of the collision of a magnetized anisotropic pulsar wind with the circumbinary environment under the approximation of an axisymmetric ideal MHD flow. The magnetic field in the pulsar wind was assumed to be toroidal, with strength depending on the distance to the pulsar, r , and the polar angle, θ : $B_\varphi \propto \sin\theta/r$. The simulations were performed for three equatorial magnetizations of the pulsar wind: $\sigma = 0.5, 0.6$, and 0.8 , and extend the study by [Bogovalov et al. \(2012\)](#) for the range of $\sigma \leq 0.1$. While in the case of small wind magnetization, $\sigma \leq 0.1$, the magnetic field has a minor impact on the plasma dynamics ([Bogovalov et al. 2012](#)), in the newly considered regime the influence of the magnetic field appears to be considerable. The opening cone in which the shocked pulsar wind propagates increases with growth of the wind magnetization. This effect can be explained as the impact of the Lorentz force that collimates the part of the flow below the current sheet and expands the part that is above (see Fig. 5). This finding has an important implication for scenarios that aim to explain the origin of the bright GeV flares detected with *Fermi* LAT from PSR B1259. Since the registered gamma-ray luminosity exceeds the pulsar spin-down luminosity, the production of the gamma-ray emission in highly collimated outflows seems to be the most plausible scenario. Our simulations show that in the considered regime, $\sigma \sim 1$, the magnetic pinch results in de-collimation of the outflow. This makes scenarios relaying on a large Doppler boosting to be less feasible and the overall interpretation of the GeV flares to be even more challenging.

ACKNOWLEDGMENTS

The authors thank V.Bosch-Ramon, M.V.Barkov, and referee, Barbara Olmi, for their useful comments. The work of S.Bogovalov was supported by the Ministry of Education and Science of the Russian Federation, MEPhI Academic Excellence Project (contract №02.a03.21.0005, 27.08.2013) and by RFBR grant №16-02-00822/18. DK is supported by JSPS KAKENHI Grant Numbers JP18H03722, JP24105007, and JP16H02170. AVK acknowledges support by RFBR 18-02-00907.

REFERENCES

- Abdo A. A., et al., 2010, *ApJ*, **723**, 649
- Abdo A. A., et al., 2011, *ApJ*, **736**, L11
- Abeysekara A. U., et al., 2018, *Nature*, **562**, 82
- Abramowski A., et al., 2013, *A&A*, **551**, A94
- Aharonian F., et al., 2005, *A&A*, **442**, 1
- Aharonian F., et al., 2009, *A&A*, **507**, 389
- Bandiera R., 1993, *A&A*, **276**, 648
- Barkov M. V., Bosch-Ramon V., 2016, *MNRAS*, **456**, L64

- Barkov M. V., Bosch-Ramon V., 2018, *MNRAS*, **479**, 1320
- Barkov M. V., Lyutikov M., Khangulyan D., 2019a, *MNRAS*, **484**, 4760
- Barkov M. V., Lyutikov M., Klingler N., Bordas P., 2019b, *MNRAS*, **485**, 2041
- Bogovalov S. V., 1999, *A&A*, **349**, 1017
- Bogovalov S. V., Khangoulia D. V., 2002, *MNRAS*, **336**, L53
- Bogovalov S., Tsinganos K., 1999, *MNRAS*, **305**, 211
- Bogovalov S. V., Chechetkin V. M., Koldoba A. V., Ustyugova G. V., 2005, *MNRAS*, **358**, 705
- Bogovalov S. V., Khangulyan D. V., Koldoba A. V., Ustyugova G. V., Aharonian F. A., 2008, *MNRAS*, **387**, 63
- Bogovalov S. V., Khangulyan D., Koldoba A. V., Ustyugova G. V., Aharonian F. A., 2012, *MNRAS*, **419**, 3426
- Bordas P., Yang R., Kafexhiu E., Aharonian F., 2015, *ApJ*, **807**, L8
- Bordas P., et al., 2017, in 6th International Symposium on High Energy Gamma-Ray Astronomy. p. 040017 ([arXiv:1610.03264](https://arxiv.org/abs/1610.03264)), [doi:10.1063/1.4968921](https://doi.org/10.1063/1.4968921)
- Bosch-Ramon V., Barkov M. V., 2011, *A&A*, **535**, A20
- Bosch-Ramon V., Barkov M. V., Khangulyan D., Perucho M., 2012, *A&A*, **544**, A59
- Bosch-Ramon V., Barkov M. V., Perucho M., 2015, *A&A*, **577**, A89
- Bosch-Ramon V., Barkov M. V., Mignone A., Bordas P., 2017, *MNRAS*, **471**, L150
- Böttcher M., Dermer C. D., 2005, *ApJ*, **634**, L81
- Caliandro G. A., Cheung C. C., Li J., Scargle J. D., Torres D. F., Wood K. S., Chernyakova M., 2015, *ApJ*, **811**, 68
- Chang Z., Zhang S., Chen Y.-P., Ji L., Kong L.-D., Liu C.-Z., 2018, *Research in Astronomy and Astrophysics*, **18**, 152
- Chernyakova M. A., Illarionov A. F., 1999, *MNRAS*, **304**, 359
- Chernyakova M., Neronov A., Lutovinov A., Rodriguez J., Johnston S., 2006, *MNRAS*, **367**, 1201
- Chernyakova M., Neronov A., Aharonian F., Uchiyama Y., Takahashi T., 2009, *MNRAS*, **397**, 1232
- Chernyakova M., et al., 2014, *MNRAS*, **439**, 432
- Chernyakova M., et al., 2015, *MNRAS*, **454**, 1358
- Corbet R. H. D., et al., 2016, *ApJ*, **829**, 105
- Corbet R. H. D., et al., 2019, *arXiv e-prints*, p. [arXiv:1908.10764](https://arxiv.org/abs/1908.10764)
- De Becker M., Rauq F., 2013, *A&A*, **558**, A28
- Del Zanna L., Amato E., Bucciantini N., 2004, *A&A*, **421**, 1063
- Dougherty S. M., Pittard R. J. M., O'Connor E. P., 2005a, in Rauw G., Nazé Y., Blomme R., Gosset E., eds, *Massive Stars and High-Energy Emission in OB Associations*. pp 49–52 ([arXiv:astro-ph/0510538](https://arxiv.org/abs/astro-ph/0510538))
- Dougherty S. M., Beasley A. J., Claussen M. J., Zauderer B. A., Bolingbroke N. J., 2005b, *ApJ*, **623**, 447
- Dubus G., 2006a, *A&A*, **451**, 9
- Dubus G., 2006b, *A&A*, **456**, 801
- Dubus G., 2013, *A&ARv*, **21**, 64
- Dubus G., Cerutti B., 2013, *A&A*, **557**, A127
- Dubus G., Cerutti B., Henri G., 2008, *A&A*, **477**, 691
- Dubus G., Cerutti B., Henri G., 2010, *MNRAS*, **404**, L55
- Eichler D., Usov V., 1993, *ApJ*, **402**, 271
- Fujita Y., Kawachi A., Akahori T., Nagai H., Yamaguchi M., 2019, *arXiv e-prints*, p. [arXiv:1904.08429](https://arxiv.org/abs/1904.08429)
- Hamaguchi K., et al., 2018, *Nature Astronomy*, **2**, 731
- Johnson T. J., Wood K. S., Kerr M., Corbet R. H. D., Cheung C. C., Ray P. S., Omodei N., 2018, *ApJ*, **863**, 27
- Johnston S., Manchester R. N., Lyne A. G., Bailes M., Kaspi V. M., Qiao G., D'Amico N., 1992, *ApJ*, **387**, L37
- Johnston S., Manchester R. N., Lyne A. G., Nicastro L., Spyromilio J., 1994, *MNRAS*, **268**, 430
- Johnston S., Manchester R. N., Lyne A. G., D'Amico N., Bailes M., Gaensler B. M., Nicastro L., 1996, *MNRAS*, **279**, 1026
- Johnston S., Ball L., Wang N., Manchester R. N., 2005, *MNRAS*, **358**, 1069
- Kalopotharakos C., Contopoulos I., Kazanas D., 2012, *MNRAS*, **420**, 2793
- Kaspi V. M., Tavani M., Nagase F., Hirayama M., Hoshino M., Aoki T., Kawai N., Arons J., 1995, *ApJ*, **453**, 424
- Kennel C. F., Coroniti F. V., 1984, *ApJ*, **283**, 710
- Khangoulia D. V., Bogovalov S. V., 2003, *Astronomy Letters*, **29**, 495
- Khangulyan D., Hnatic S., Aharonian F., Bogovalov S., 2007, *MNRAS*, **380**, 320
- Khangulyan D., Aharonian F., Bosch-Ramon V., 2008, *MNRAS*, **383**, 467
- Khangulyan D., Aharonian F. A., Bogovalov S. V., Ribó M., 2012, *ApJ*, **752**, L17
- Khangulyan D., Bogovalov S. V., Aharonian F. A., 2014, in International Journal of Modern Physics Conference Series. p. 1460169, [doi:10.1142/S2010194514601690](https://doi.org/10.1142/S2010194514601690)
- Khangulyan D., Bosch-Ramon V., Uchiyama Y., 2018, *MNRAS*, **481**, L455
- Kirk J. G., Ball L., Skjæraasen O., 1999, *Astroparticle Physics*, **10**, 31
- Koldoba A. V., Ustyugova G. V., Bogovalov S. V., 2019, *Mathematical Models and Computer Simulations*, **11**, 86
- Kong S. W., Cheng K. S., Huang Y. F., 2012, *ApJ*, **753**, 127
- Lamberts A., Fromang S., Dubus G., Teyssier R., 2013, *A&A*, **560**, A79
- Leser E., et al., 2017, International Cosmic Ray Conference, **35**, 717
- López-Oramas A., et al., 2018, *International Journal of Modern Physics D*, **27**, 1844010
- Lyne A. G., Stappers B. W., Keith M. J., Ray P. S., Kerr M., Camilo F., Johnson T. J., 2015, *MNRAS*, **451**, 581
- Maier G., VERITAS Collaboration 2017, International Cosmic Ray Conference, **301**, 729
- Maraschi L., Treves A., 1981, *MNRAS*, **194**, 1P
- Martocchia A., Motch C., Negueruela I., 2005, in Burderi L., Antonelli L. A., D'Antona F., di Salvo T., Israel G. L., Pierantoni L., Tornambè A., Straniero O., eds, *American Institute of Physics Conference Series Vol. 797, Interacting Binaries: Accretion, Evolution, and Outcomes*. pp 581–584, [doi:10.1063/1.2130290](https://doi.org/10.1063/1.2130290)
- Michel F. C., 1973, *ApJ*, **180**, 207
- Miller-Jones J. C. A., et al., 2018, *MNRAS*, **479**, 4849
- Moldón J., Johnston S., Ribó M., Paredes J. M., Deller A. T., 2011, *ApJ*, **732**, L10
- Murata K., Tamaki H., Maki H., Shibazaki N., 2003, *PASJ*, **55**, 473
- Negueruela I., Ribó M., Herrero A., Lorenzo J., Khangulyan D., Aharonian F. A., 2011, *ApJ*, **732**, L11
- Okazaki A. T., Nagataki S., Naito T., Kawachi A., Hayasaki K., Owoc S. P., Takata J., 2011, *PASJ*, **63**, 893
- Olmi B., Bucciantini N., 2019, *MNRAS*, **484**, 5755
- Olmi B., Del Zanna L., Amato E., Bucciantini N., Mignone A., 2016, *Journal of Plasma Physics*, **82**, 635820601
- Pavlov G. G., Chang C., Kargaltsev O., 2011, *ApJ*, **730**, 2
- Pavlov G. G., Hare J., Kargaltsev O., Rangelov B., Durant M., 2015, *ApJ*, **806**, 192
- Porth O., Komissarov S. S., Keppens R., 2014, in International Journal of Modern Physics Conference Series. p. 1460168, [doi:10.1142/S2010194514601689](https://doi.org/10.1142/S2010194514601689)
- Reitberger K., Kissmann R., Reimer A., Reimer O., 2014, *ApJ*, **789**, 87
- Reitberger K., Reimer A., Reimer O., Takahashi H., 2015, *A&A*, **577**, A100
- Romero G. E., Okazaki A. T., Orellana M., Owoc S. P., 2007, *A&A*, **474**, 15
- Shannon R. M., Johnston S., Manchester R. N., 2014, *MNRAS*, **437**, 3255
- Tavani M., Arons J., Kaspi V. M., 1994, *ApJ*, **433**, L37

- Uchiyama Y., Tanaka T., Takahashi T., Mori K., Nakazawa K., 2009, [ApJ](#), **698**, 911
- Wilkin F. P., 1996, [ApJ](#), **459**, L31
- Wilkin F. P., 2000, [ApJ](#), **532**, 400
- Xing Y., Wang Z., Zhang X., Chen Y., Jithesh V., 2019, [ApJ](#), **872**, 25
- Zabalza V., Bosch-Ramon V., Aharonian F., Khangulyan D., 2013, [A&A](#), **551**, A17
- Zanin R., Fernández-Barral A., de Oña Wilhelmi E., Aharonian F., Blanch O., Bosch-Ramon V., Galindo D., 2016, [A&A](#), **596**, A55
- Zdziarski A. A., et al., 2018, [MNRAS](#), **479**, 4399
- de la Cita V. M., Bosch-Ramon V., Paredes-Fortuny X., Khangulyan D., Perucho M., 2017, [A&A](#), **598**, A13
- van Soelen B., Väisänen P., Odendaal A., Klindt L., Sushch I., Meintjes P. J., 2016, [MNRAS](#), **455**, 3674